Michael G. Waddell (mwaddell@esri.esri.sc.edu, 803-777-5905)
William Domoracki (bdomorac@esri.esri.sc.edu, 803-777-0178)
Tom J. Temples (ttemples@esri.esri.sc.edu, 803-777-3014)

NON-INVASIVE DETERMINATION OF THE LOCATION AND DISTRIBUTION OF FREE-PHASE DENSE NON-AQUEOUS PHASE LIQUIDS (DNAPLS) BY SEISMIC REFLECTION TECHNIQUES

1.0 INTRODUCTION

Current technology for the evaluation and remediation of contaminated soil and groundwater is inadequate to meet mandated cleanup levels in a cost-effective and environmentally acceptable manner. More must be learned before realistic cleanup strategies can be developed. The technology gap comes from incomplete knowledge about the subsurface geohydrology within which various remediation technologies are applied and the inability to adequately characterize movement of pollutants. The path of contaminant movement is complex because of the interaction between earth materials and contaminants that may represent the subsurface.

2.0 OBJECTIVE

Determining the location and distribution of subsurface dense nonaqueous phase liquid (DNAPL) contamination poses specific challenges. Because DNAPLs are denser than groundwater migration of these fluids in the subsurface is controlled in part by gravity. The direction of contaminant flow is not necessarily the same as groundwater flow. Below the water table DNAPLs tend to accumulate in highly concentrated discrete layers or pools in structural lows or "sinks" above low permeability geologic layers. The occurrence of DNAPL in the subsurface can be highly localized and can occur at differing structural levels. The key to maximizing the amount of DNAPL recovered from the subsurface is constructing a comprehensive and detailed picture of the geometry and spatial variations of the lithologic units comprising the subsurface. In addition, direct detection of DNAPL itself by non-invasive techniques will greatly aid remediation efforts.

Traditional methods used to determine the location and extent of DNAPL contamination require point-source data obtained from invasive methods such as borehole geophysical logs or cone penetrometer data. These invasive methods not only run the risk of cross-contamination of an aquifer, but may not locate pools of contamination due to inadequate spatial coverage.

3.0 APPROACH

The seismic reflection method provides a non-invasive means to acquire spatially dense subsurface information. Typically, a two dimensional high resolution seismic reflection survey may have data points

only a foot apart. A three dimensional seismic reflection survey, because of the greater cost involved, may have data points every 5 feet throughout a regular grid. Vertical resolution of high resolution seismic reflection surveys is three to five feet. These data, combined with existing borehole information, can provide a detailed picture of the subsurface.

In addition to providing a detailed structural picture of the subsurface, seismic data if properly calibrated with borehole information, can be used to map aquifer properties such as porosity, permeability, and clay content. This information when integrated into two and three dimensional structural models can delineate preferential pathways for subsurface contaminant transport. Under certain circumstances, borehole calibrated seismic reflection data can be used to infer the presence of a specific fluid within a lithologic unit. These techniques utilize the fact that a change in the fluid content within a lithologic unit causes change in the recorded seismic amplitude as a function of the angle of incidence of the impinging energy, i.e. the source to receiver offset distance. In the Petroleum industry these reflection amplitude-versus-offset (AVO) techniques have been used successfully for over ten years to directly detect the presence of subsurface hydrocarbons (Ostrander, 1984; Allen and Peddy, 1993). Recently, we have used this method to delineate free phase DNAPL concentrations at a depth of 150 feet at the Savannah River Site (Waddell et al., 1997).

4.0 PROJECT DESCRIPTION

Seismic reflection surveying has been used since the mid-1920s to map subsurface geology primarily for petroleum exploration (see Waters, 1981 for an overview). However, use of the method for engineering and environmental applications did not begin in earnest until the early 1980s. The principles of reflection seismology are the same for both the petroleum and environmental fields. The major difference is scale.

In the 1960's petroleum companies recognized that in young sediments (Tertiary age) large seismic amplitudes were associated with gas saturated sands. It was soon realized, however, that not all large seismic amplitudes represented hydrocarbon saturated sands. The normal incidence (NI) reflectivity (bright spot) techniques involved three different scenarios base upon a water saturated state and a hydrocarbon saturated state (for this discussion a sand/shale or sand/clay interface). The scenarios are classified by changes in NI reflectivity from a water saturated a gas or hydrocarbon sand.

The three scenarios are:

- Dim spot- a large positive amplitude that is reduced to a smaller positive amplitude,
- Phase reversal- a small positive amplitude that changes to small negative amplitude and
- Bright spot- a negative amplitude increasing to a large negative amplitude.

The dim spot is generally associated with a large acoustic impedance contrast and is a good technique for inferring lithology. Bright spot anomalies are generally good for interpreting lithology and estimating sand thickness. Phase reversal reflections are not generally reliable because geologic features (i.e. faults) can cause the reflections toappear to reverse phase. This does not necessarily indicate a change lithology (Vern and Hilterman, 1995). The bright spot technique was the first direct hydrocarbon indicator.

In 1984 Ostrander published a article entitled "Plane-wave reflection coefficients for gas sands at non-normal angles of incidence". Ostrander observed that the P-wave reflection coefficient at the interface between two media varies with the angle of incidence of the impinging energy. In this article Ostrander investigated the phenomenon of compressional wave reflection amplitude variation with angle of incidence and changes in Poisson's ratio.

Much of Ostrander's work was based upon Koefoed's, 1955 work determining the reflection coefficients of plane longitudinal waves reflected at a boundary between two elastic media. Koefoed observed that if there were two elastic media with the top medium having a smaller Poisson's ratio than the underlying medium, there would be an increase in the reflection coefficient with increasing angle of incidence. He also observed that if Poisson's ratio of the lower medium was lower than the overlying medium, the opposite would occur with a decrease in the reflection coefficient with an increase in the angle of incidence. Another observation was that the relative change in reflection coefficient increases as the velocity contrast between the two media decreases. Koefoed also observed that if Poisson's ratio for both media was increased but kept equal, the reflection coefficient at the larger angles of incidence would also increase. Ostrander (1984) observed that changes in Poisson ratio caused by the presence of hydrocarbons in the pore space had dramatic effect on the P-wave reflection coefficients and that these effects could be related to seismic amplitude anomalies.

AVO analysis involves comparing modeled responses with field data to find a deviation from an expected background response. The expected background response is usually taken to be a water saturated reservoir.. DNAPLs have the same acoustic characteristics as liquid hydrocarbons. If DNAPL is present in free phase in large enough quantities, similar types of analyzes as those performed by the petroleum industry can be applied to directly detect the presence of DNAPL.

An understanding of reflection AVO techniques can be obtained by a review of elastic wave propagation. A P-wave incident on a boundary between two linear elastic homogeneous isotropic (LEHI) media generates four types of waves: 1) transmitted P-wave; 2) reflected P-wave; 3) reflected S-wave; 4) a transmitted S-wave (Figure1). The amplitudes of the reflected and transmitted waves at the boundary depend upon the P-wave and S-wave velocities, the density of the two media, and the angles of incidence and refraction, as determined from Snell's Law.

The variation of the reflection and transmission coefficients with incident angle and source to receiver offset is referred to as offset-dependent-reflectivity (Castagna and Backus, 1993). The values of the reflection and transmission coefficients for non-normal angles of incidence are given by the Zoeppritz (1919) equations. The complexity of the Zoeppritz equations has led to numerous approximations to simplify the calculations. Some of the approximations are Bortfield (1961), Aki and Richards (1980), and Shuey 1985.

In this study, we used the Shuey modification of Zoeppritz equations to express the angle dependent reflectivity in terms of P-wave Velocity, bulk density, and Poisson's ratio. The Shuey approximation of Zoeppritz's equations stresses the importance of Poisson's ratio as the primary determinant of the AVO

response of a reflection (Allen and Peddy, 1993). The formula for the reflection coefficient (amplitude) is:

$$R? \,.\, R_0 \% (A_O \,(\, R_O \% \frac{? s}{1 \& s^2}) \,(\, \sin^2 ? \% \frac{1}{2} \,(\, \frac{? V_p}{V_p} \,(\, \tan^2 ? \& \sin^2 ?$$

$? V_p = (V_{p2} - V_{p1})$ $\quad$ $? = (?_2 + ?_1) / 2$

$V_p = (V_{p2} + V_{p1}) / 2$ $\quad$ $? s = (s_2 + s_1)$

$? V_s = (V_{s2} - V_{s1})$ $\quad$ $s = (s_2 + s_1) / 2$

$V_s = (V_{s2} + V_{s1}) / 2$

$? ? = (?_2 - ?_1)$ $\quad$ $? = (?_2 + ?_1) / 2$

$$R_o \,.\, \frac{1}{2} \left(\frac{? V_p}{V_p} \% \frac{? ?}{?} \right) \qquad A \,' A_0 \% \left(\frac{1}{(1 \& s)^2} \right) \frac{? s}{R_0}$$

$$A_0 \,' B \& 2 \left(1 \% B \right) \left(\frac{1 \& 2s}{1 \& s} \right) \qquad B \,' \frac{\frac{? V_P}{V_p}}{\frac{? V_p}{V_p} \% \frac{? ?}{?}}$$

V_{p1}= P-wave velocity of layer one $\quad$ V_{p2}= P-wave velocity of layer two
V_{s1}= S-wave velocity of layer one $\quad$ V_{s2}= S-wave velocity of layer two
$?_1$ = Density of layer one $\quad$ $?_2$ = Density of layer two
s_1 = Poisson Ratio of layer one $\quad$ s_2 = Poisson Ration of layer two
$?_1$ = incidence and transmission angle layer one.
$?_2$ = incidence and transmission angle layer two.
R_0 = Normal incidence (NI), i.e. reflection coefficient for zero-offset.
B = is the AVO gradient.

A_0= is the normal incidence amplitude.

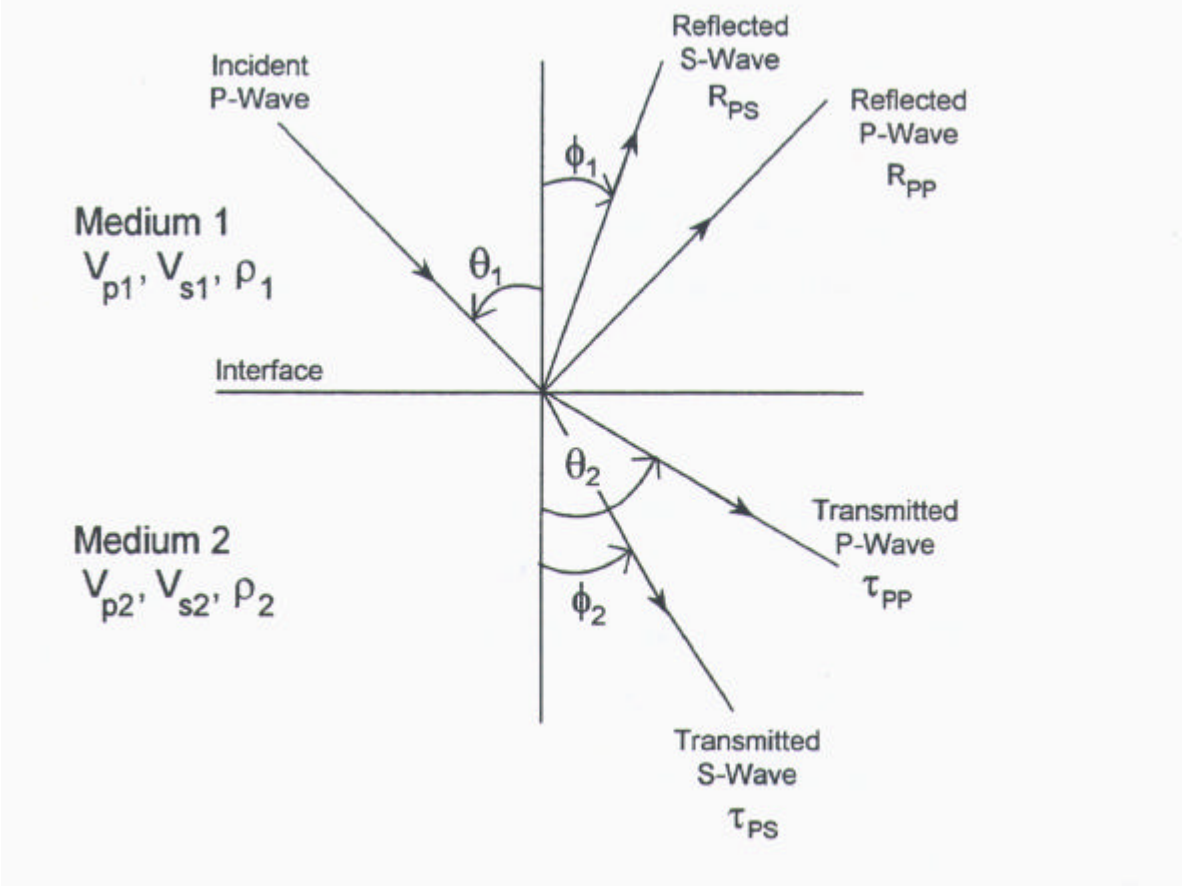

Figure 1. Elastic waves generated at a boundary. A P-wave incident at a angle q on a boundary between two linear elastic homogenous isotropic (LEHI) materials generates four wave types: reflected P, reflected S, transmitted P, transmitted S. The angles of reflection and refraction are governed by Snell=s law from optics. The material properties of the media are described by the P-wave velocity, , density, , and Poisson's ratio. The S-wave velocity can be found from the P-wave velocity and Poisson's ratio.

Reflection AVO can be thought of a combination of normal incidence reflectivity and a far offset reflectivity, or "Poisson reflectivity", that arises primarily as a result of changes in the Poisson's ratio between media.

5.0 RESULTS

Savannah River Site

At the M-Area seepage basin there are two primary types of DNAPLs present below the water table, trichloroethylene (TCE) and tetrachloroethylene (PCE).

Two methods were used to investigate any AVO effects caused by the presence of DNAPL. If the models are correct, no significant change in amplitude would exist under 22^0 caused by the presence of DNAPL. If DNAPL is present, however a significant amplitude effect would be noted offsets with angles of incidence over 22^0. Method one was the range limited stacking. Instead of gathering and stacking the data using the full range of offsets, the seismic data were stacked using subsets of ranges.

The near offsets are gathered and stacked and the far offsets were gathered and stacked. The offset range limited stacks were produced using the Hampson-Russell *Amplitude Versus Offset Analysis* software and plotted in an amplitude envelope color attribute format, which enhances AVO anomalies. The second AVO analysis technique used was the Smith and Gidlow "Fluid Factor" stack (Smith and Gidlow, 1987). The "Fluid Factor" stack is derived from the Aki and Richards (1980) approximation of Zoeppritz equations and the Castagna, Batzle and Eastwood (1985) "mudrock line" for 100% water saturated clastic silicate rocks. Using the "mudrock line" and the Aki and Richards approximation a model is generated with the available velocities from deriving a series of weighting factors (multiplying factors) that are time and space variant. The weighting factors are then applied to the CDP gathers after NMO (normal moveout). If the model is valid, the amplitudes of the CDP stack will be zero for 100% water saturated clastic sediments. Any residual reflections should denote sediments saturated with fluids other than water. In this project, DNAPL would be the only fluid other than water to saturate or partially saturate the sediments.

Limited Offset Range Stacks M-1

Figure 2 is the near offset stack (offsets from 20 to 57 feet) and the far offset stack (offsets from 58 to 114 feet). Line M-1 is located in such a manner so that the line crosses over a known pool of DNAPL. The DNAPL was bailed from well MSB-3D from an approximate depth of 155 feet below land surface. Any anomalies associated with the presence of DNAPL would appear only on the far offset stack. On line M-1 there appeared to be three major anomalies and two minor ones. The first anomaly located near CDP 619 at approximately 110 ms, is where wells MSB-22 and MSB-3D are located. This anomaly is located at the depth and location of the known "pool" of free phase DNAPL. On the near offset stack section the anomaly is absent. The second anomaly at CDP 171 at approximately 90 ms is present on the far offset stack, but absent on the near offset stack (Fig.2). The location and position of this anomaly, 90 ms, indicates that it is above the water table. The water table in this area occurs at approximately 100 ms on the seismic data (120 feet BLS). Well MOX-6 was drilled on the anomaly and DNAPL was encountered at 90 feet below land surface in sediments that had a soil concentration of 10.9 ppm (parts per million) PCE and TCE with an aqueous concentration of 3.066 ppm. There also appears to be another anomaly near CDP 859 (Fig. 2) at approximately 110 ms present on the far offset stack, but absent on the near offset stack.

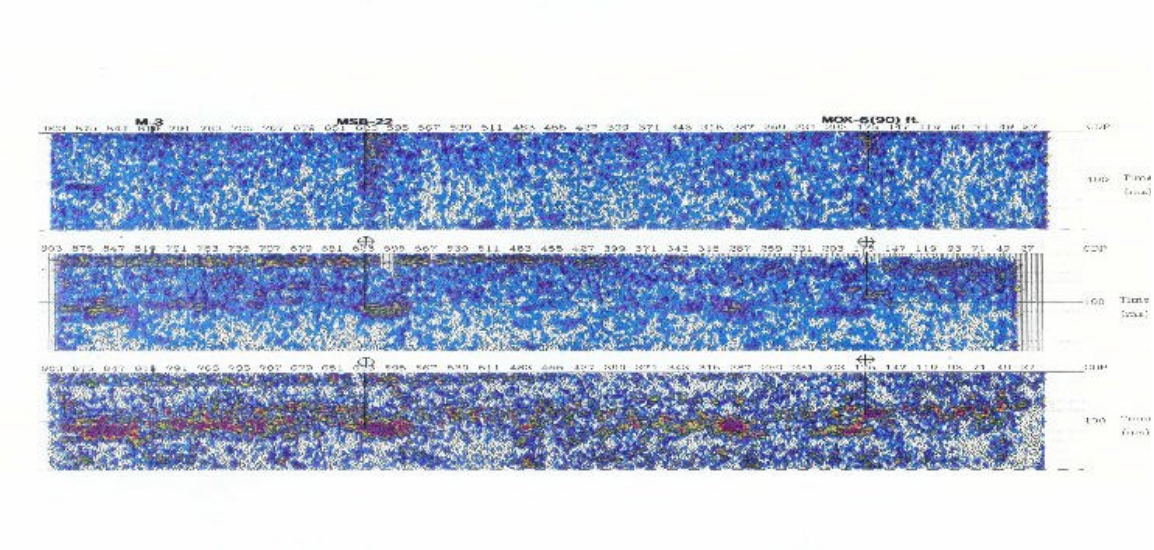

Figure 2. Range limited and Smith and Gidlow Fluid Factor Stack for line M-1

M-2 Range Limited Offset Stack

After the processing and AVO analysis of line M-1, a decision was made to acquire two additional lines. The location of M-2 was based upon the results of a contaminant transport model that indicated the direction of DNAPL movement in the subsurface. The M-Area is a notoriously low signal to noise ratio seismic area. Therefore, it was decided to increase the number of channels, increasing the CDP fold, thereby increasing the signal to noise ratio. The geometry parameters were based upon the same modeling results, i.e. half the receivers with offsets under 22^0 angle of incidence and half with offsets over 22^0 angle of incidence. Figure 3 contains the range limited offset stacks for line M-2. The near offset stack ranged from 29 to 88 feet and the far offset stack ranged from 88 to 175 feet (Fig. 3). There is a large anomaly at approximately 110 ms on the far offset stack beginning at CDP 244 and continuing to CDP 460 (Fig.3). Comparison of this stack with the near offset stack shows the anomaly to be mostly absent. Well MRS-2 was drilled near CDP 436 (Fig. 3). The concentration of DNAPL was in parts per million (ppm) at the depth of the anomaly. Based on the far offset stack, well MRS-2 appears to have missed the major anomaly and is instead located on the flank of the large anomaly. Another anomaly is located near CDP 590 (Fig. 3) at about 115 ms. This particular anomaly occurs deeper at or near the base of the channel. Preliminary evidence suggests that most of the channel is filled with clay however portions of the channel are sand filled, e.g. point bars. The location of this anomaly suggests, that the DNAPL has migrated downward through the porous point bar deposits. The final anomaly is located from CDP 676 to 730 at approximately 110 ms. Well MOX-1 was drilled slightly off line M-2 where DNAPL was encountered in over 100 ppm concentration from 138 feet to 144 feet.

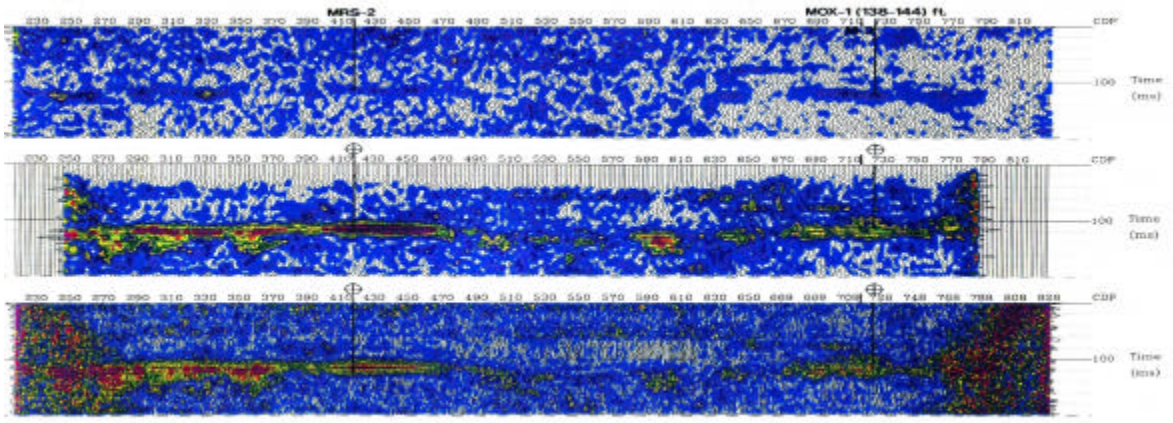

Figure 3. Range limited and Smith and Gidlow Fluid Factor Stack for line M-2

M-1 (FFS)

Using the Smith and Gidlow fluid factor analysis, a fluid factor stack was generated(Fig.2). As on the limited offset stack, three primary anomalies are present. The anomaly near CDP 619 at 110 ms is pronounced. The other anomaly near CDP 171 at 90 ms has been tested with the drilling of well MOX-6. The combined concentration of TCE and PCE in the soil is 10.9 ppm (parts per million) and the aqueous combined concentration is 3.066 ppm. An anomaly between CDPs 299 and 315 is also present. The anomaly at CDP 619 at 110 ms is very pronounced, and is the location of the known DNAPL in well MSB-3 and MSB-22. The other large anomaly near CDP 859 at approximately 110 ms.

M-2 (FFS)

On the fluid factor stack(FFS) (Fig.3) the major anomalies identified on the far offset stack are present. A large continuous anomaly is located from CDP 244 to 460 at 110 ms. A deeper anomaly exists at CDP 590 at 115 ms. The MOX-1 well was drilled into the anomaly at CDP 676-730 (Fig. 3). On either end of the FFS there appears to be anomalies starting at the surface and extending downward at an angle. This phenomenon is the result of stacking coherent noise, such as surface waves or groundroll, during processing of the data. The FFS indicates that the thickness of the DNAPL anomaly is larger than on the far limited offset stack. This is especially true at CDP 590 (Fig.3) and at CDP 308.

Phase one of the interpretation was to determine which reflectors correspond to the Plio/Pleistocene and the Caliche zone. The significance of these reflectors is that the DNAPL tends to accumulate in the vicinity of these two events in the subsurface. A VSP was acquired in well 299-W15-32 (Fig. 4) to establish a tie between the geologic units and the seismic events present in the survey data. The data was acquired using a 96-channel Geometrics Strataview recording system Lines were laid to tie wells in the vicinity of the crib (Fig.4) with high concentrations of CCl_4

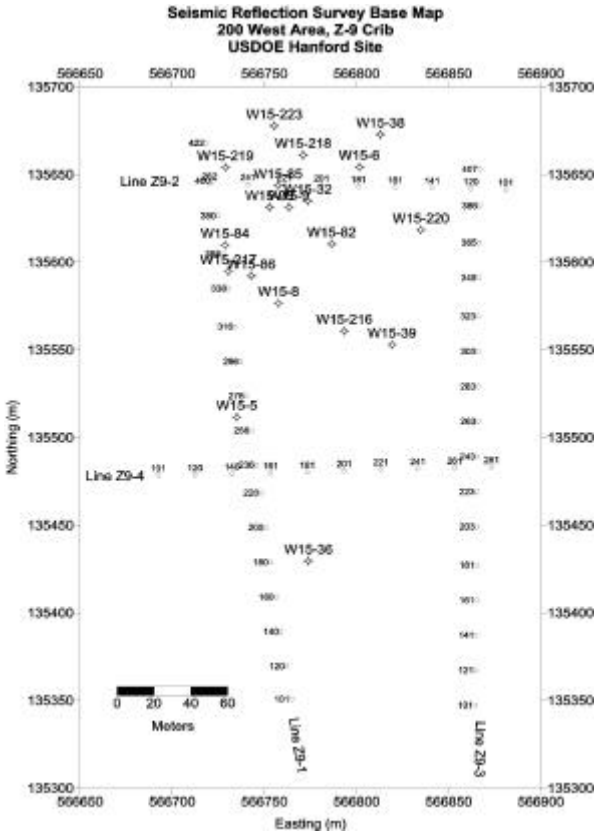

Figure 4. Location plat for the Hanford 200 W area.

Structural Interpretation

Structure contour maps were generated on two horizons, the Plio/ Pleistocene (green event, and the top of Caliche (blue event). The channel downcutting into the Plio/Pleistocene surface is readily apparent on the structure contour map on top of the Plio/Pleistocene(Fig. 5). A structural high is located on line Z-9-1 at SP 340. The surface dips off to the north and northeast from this high. A structural high also exists on the southern end of Line Z-9-3. Most of the relief on this surface is from the erosion by the channel in the overlying unit bisecting the map area. The movement of DNAPL in the subsurface is more dependent on structure than groundwater flow. Given the

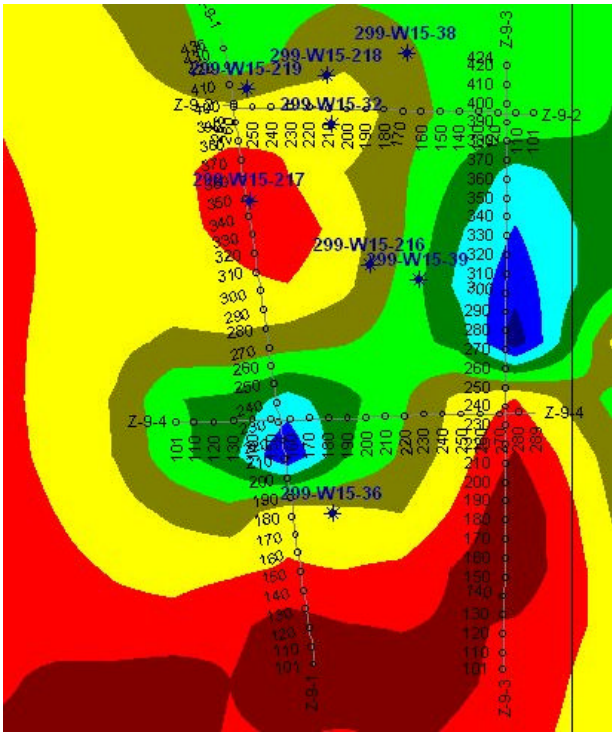

Figure 5. Structure contour map in time on the Plio/Pleistocene.

location of the source of entry for the solvents into the ground, the most likely flow direction for DNAPL would be to the north and northeast of the Plio/Pliestocene high present on line Z-9-1 (Fig. 5).

A similar structural picture is observed on the Top of Caliche map (Fig.6). A structural high exists on line Z-9-1 near the tie with Line Z-9-2. The geologic characteristics of this surface would indicate that this would be the most likely candidate surface for the DANPL to collect. Any DNAPL flowing along this surface, assuming that crib is the source would gravity flow to the north and northeast.

DIRECT DETECTION OF DNAPL

At the 200 W Area the DNAPL present consists of carbon tetrachloride (CCl_4). The solvent is present both in the vadose zone as well as in the water table. Carbon tetrachloride is found throughout the 65-meter thick vadose zone (Rohay, 1994). Rohay (1994) states that the highest concentrations of CCl_4 are associated with the Hanford fine and the Plio-Pleistocene units located approximately 35-40 meters below ground surface.

Based upon the modeling for this report an amplitude anomaly should be present along the Plio/Pleistocene and top of Caliche horizons where DNAPL is present. Each line was taken through a standard processing

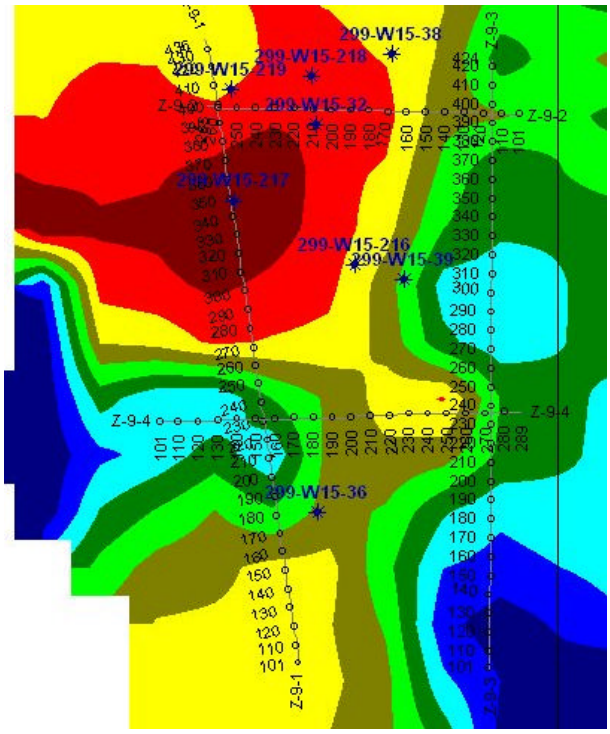

Figure 6. Structure Contour map in time on Top of Caliche.

scheme to generate the sections used for structural interpretation. To enhance the amplitude increase due to the presence of DNAPL an additional processing step was taken.

Each line was processed to enhance amplitude increases. Taking each trace and raising the amplitude values by 10 to the ith power of the trace accomplished this. In effect this step had the effect of boosting the high amplitude data exponentially while suppressing the low amplitude values. This enhancement suppressed the amplitude of the events where no DNAPL was present and increased the amplitude of the reflecting horizon where CCl_4 is present.

Z-9-1 Enhanced Amplitude Stack

Figure 7 is the enhanced amplitude stack for Z-9-1. Significant amplitude anomalies exist on line Z-9-1 along the Top of Caliche event. An anomaly exists from SP 379-426 at 121 ms, from SP 346-360 at 123 ms and from SP 270 –306 at 125 ms. A minor anomaly exists from SP 128-164 at 123 ms. Amplitude increases are seen in the interval between the Plio/Pleistocene (green event) and the Caliche (blue event) boundaries.

According to Rohay, (1994) well 299-W15-217 had the highest measured CCl_4 concentrations present

in the subsurface of the area (37,817 ppb) at a depth of 34.7 meters, the Plio/Pleistocene event (green). This corresponds to one of the significant amplitude anomalies present on line Z-9-1 from SP 346-360 at approximately 120 ms (Fig.7).

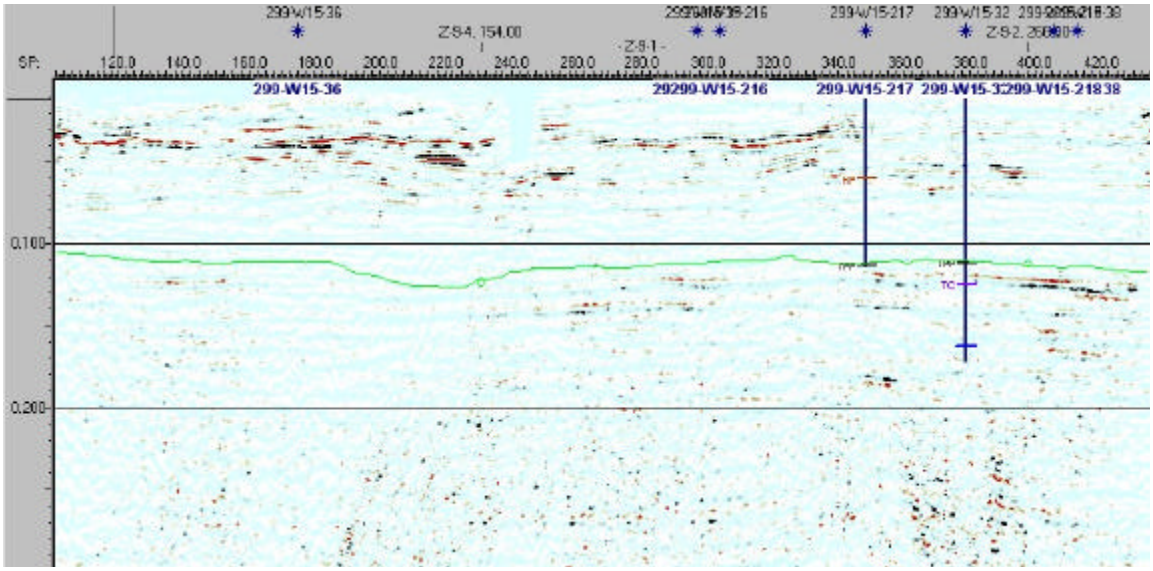

Figure 7. Enhanced amplitude plot of Line Z-9-1. Areas in black are positive amplitudes, areas in red are negative amplitudes. Green Horizon is top of Plio/Pleistocene

Z-9-2

Figure 8 is the enhanced amplitude stack for Z-9-2. Significant amplitude increases exist on Z-9-2 from SP 114-152, SP 154-219 and SP 226-261 at approximately 127 ms. This corresponds to near the top of Caliche reflector. Amplitudes in general are significantly higher along this profile and are vertically more extensive than on Z-9-1. These amplitudes along with the aerial extent suggest that significant DNAPL is present along this surface.

Well 299-W15-218 projects into an amplitude anomaly on Line Z-9-2 at SP 209 and well 299-W15-219 projects into the end of an anomaly on Z-9-2 at SP 260. Wells 299-W15-218 and 299-W15-219 yielded CCl_4 concentrations of 15,794 ppb at 33.5 m and 11,688ppb at 34.9m respectively. These depths are in good agreement with line Z-9-2 for the interval between the Plio/Pliestocene and the top of Caliche reflectors.

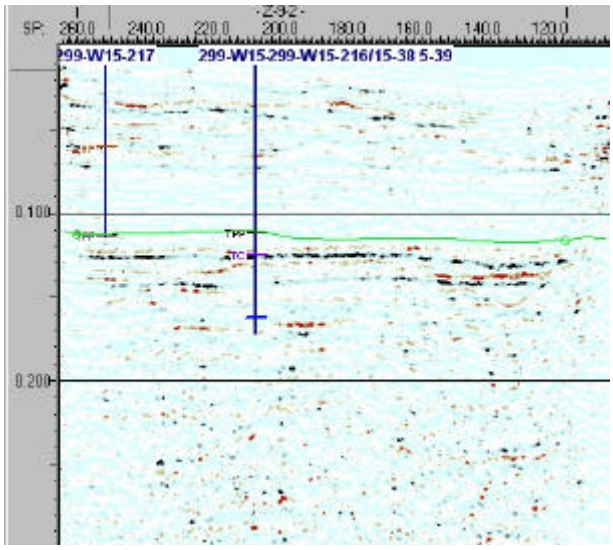

Figure 8. Enhanced amplitude plot of Line Z-9-2. Areas in black are positive amplitudes, areas in red are negative amplitudes. Green Horizon is top of Plio/Pleistocene

Z-9-3

Figure 9 is the enhanced amplitude stack for Z-9-3. Z-9-3 is located east of the crib area. A major increase in amplitude exists on Z-9-3 from SP 351-400 along the top of Caliche reflector. To the south along the line an amplitude increase exists from SP 114-204 within the Ringold Formation, but above the water table. The significance of this amplitude anomaly is not known at this time.

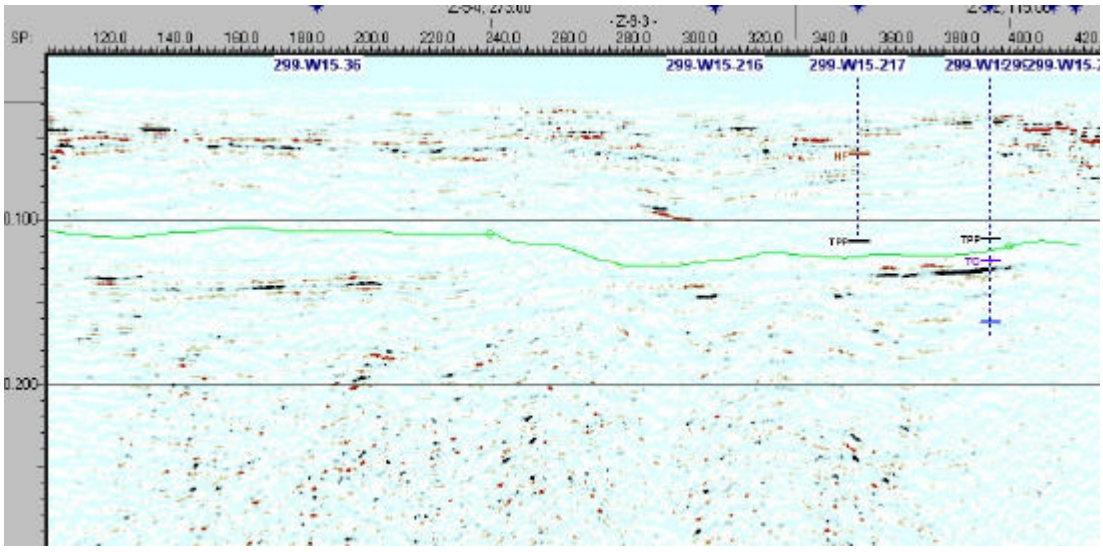

Figure 9. Enhanced amplitude plot of Line Z-9-3. Areas in black are positive amplitudes, areas in red are negative amplitudes. Green Horizon is top of Plio/Pleistocene.

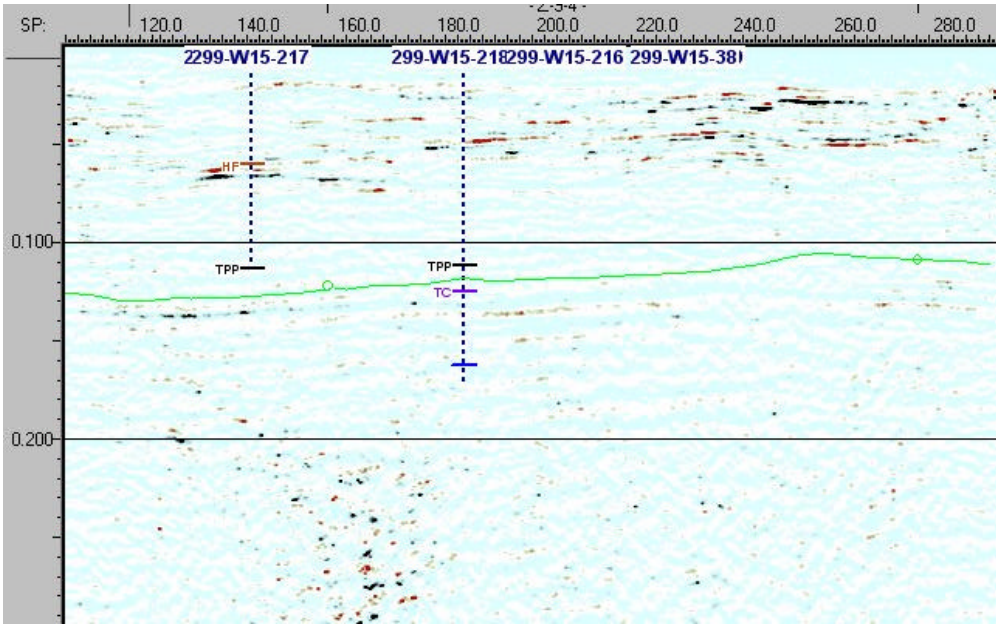

Figure 10 is the enhanced amplitude stack for Z-9-4. Areas in black are positive amplitudes, areas in red are negative amplitudes. Green Horizon is top of Plio/Pleistocene

Figure 10 is the enhanced amplitude stack for Z-9-4. The line is located to the south of the crib area. Z-9-4 displays no amplitude anomalies along the line at any horizon. This would indicate that there is no DNAPL present along the profile.

Integrated Interpretation

Plio/Pleistocene

Amplitude maps were created on two horizons, the Plio/Pleistocene and the Top of Caliche reflectors. Amplitude values along these surfaces were picked and contoured to allow interpretation of the data for DNAPL distribution.

Figure 11 is a contour map of the amplitudes at the top of the Plio/Pleistocene horizon. Modeling of this horizon shows that in the presence of CCl_4 DNAPL, the amplitude along this event should be reduced, i.e. a dim-out. Areas of dim-out are represented by the green and blue colored areas. In general, these areas are located under the crib, to the east of the crib and west of the crib. These reduced amplitude zones are located in structural lows along the surface of the Plio/Pleistocene
(Fig 5).

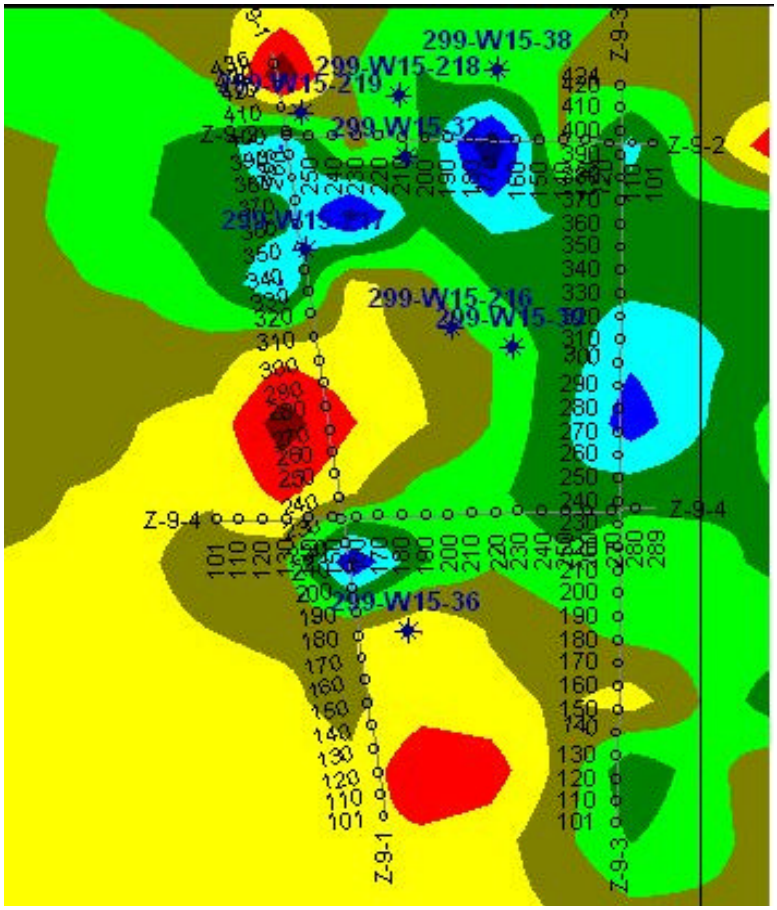

Figure 11 Contour map of amplitude values Plio/Pleistocene.

Top of Caliche

Figure 12 is the amplitude map on the top of the Caliche reflector. Based on the modeling, a high amplitude event at the top of the Caliche is associated with the presence of DNAPL. Amplitude values on the Caliche surface represented by the red and yellow are the highest along line Z-9-2 and are projected to run to the north of the area. A large area represented by the area colored green also displays an increase in amplitude over background. Under assumption that an increase in amplitude indicates DNAPL, CCl_4 in free phase has collected along the top of Caliche in this location. No evidence exists for the presence of DNAPL south and east of the crib in the area colored blue at this horizon.

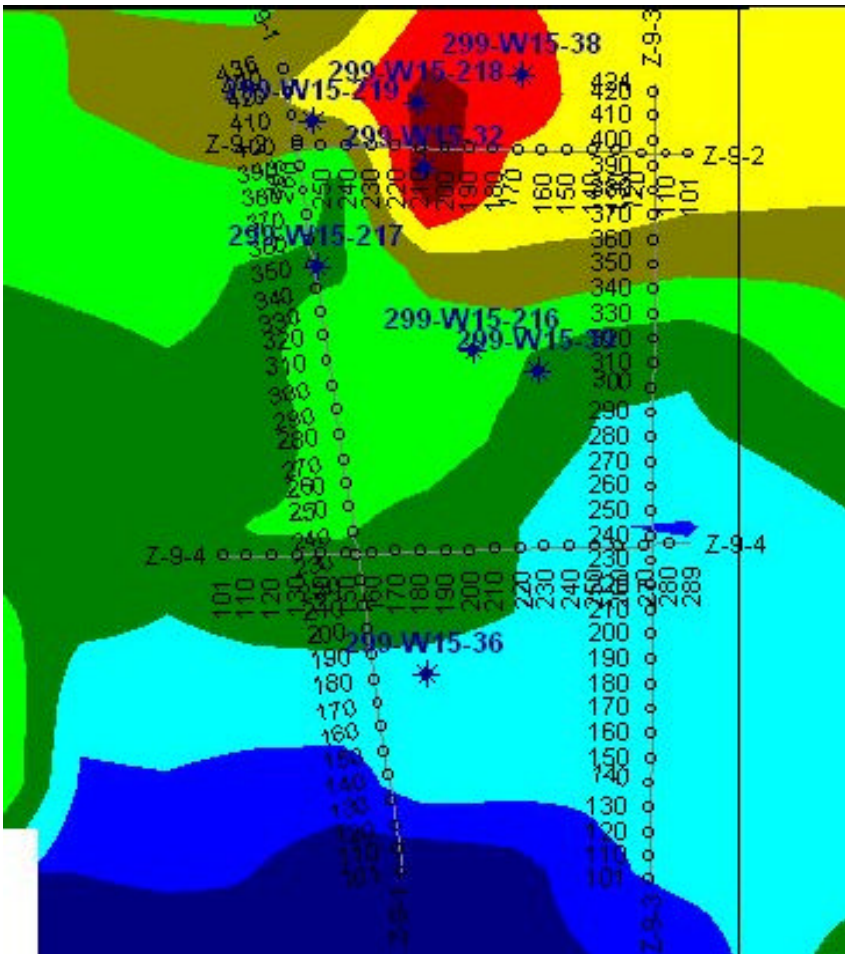

Figure.12 Contour map of the amplitude values Top of Caliche surface.

Figure 13 is a contour map of the average concentration of CCl_4 in the Plio/Pleistocene—Caliche interval in the crib area. Information from five wells, 299-W15-216, 299-W15-217, 299-W15-218, 299-W15-219, and 299-W15-220 were collected and averaged over the interval represented by the Plio/Pleistocene and gridded. Areas of high concentration of CCl_4 in the interval are represented by red values. Areas of low concentration are in shades of blue. The northwest area of the map (the area encompassing wells 299-W15-217, 299-W15-218, 299-W15-219) falls within the zone of high concentration. This agrees well with the amplitude anomaly maps of the top of Plio/Pleistocene (Fig. 5) and top of Caliche (Fig. 6). The area directly under well 299-W15-218 is an overlay on all maps.

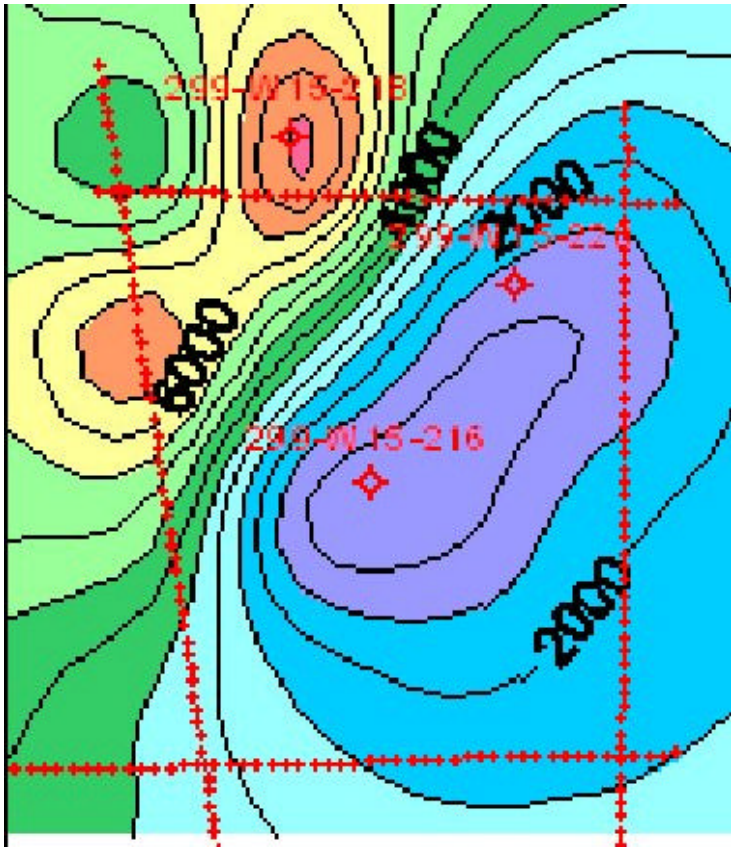

Figure 13. Contour of CCl_4 concentrations in crib area.

The seismic data showing the position of free phase CCl_4 in the subsurface agrees well with the known concentrations based on well data. Modeling results indicate that a dim out in amplitudes should be present along the top of Plio/Pleistocene event where CCl_4 with an increase in amplitude along the top of Caliche surface.

Based on the close agreement of the seismic and the well data, a prediction of the location of free phase CCl_4 can be made with reasonable confidence at the Caliche event. The event when enhanced yields a distinctive anomaly that can be mapped with high confidence.

6.0 APPLICATION

In summary, seismic reflection surveying and seismic reflection AVO analysis are noninvasive techniques that, under certain circumstances, provide a means of 1) mapping subsurface lows where DNAPL might accumulate, and 2) to directly detect the presence of free phase DNAPL in the subsurface. This approach

significantly reduces the cost of site characterization and prevents cross contamination between aquifers by reducing the number of monitoring wells.

The seismic reflection survey is the only subsurface remote sensing method capable of providing dense spatial sampling of subsurface material properties at depths 30 feet and greater. In addition, emerging technology, such as application of the AVO techniques described and proposed herein, present the possibility of directly detecting the presence of subsurface DNAPL. These technologies will result is a significantly more extensive understanding of the subsurface characteristics and properties of waste sites, which will lead to an efficient and cost-effective cleanup of groundwater.

Furthermore DNAPLs can be identified more quickly by seismic reflection surveying because of the dense subsurface sampling and direct detection potential. This information will provide a better basis for developing groundwater models used to design remediation strategies. The delineation of contaminant plumes and the placement of monitoring wells will be facilitated, thereby saving time and money over a method using the random installation of wells.

Applicationof seismic reflection techniques to subsurface site characterization will reduce public and occupational health risks because, as a noninvasive technique, there will be less exposure to hazardous subsurface contaminants. Field crews will assume less risk. There is less disturbance of aquifers and fewer opportunities for inadvertently spreading contaminants.

Site remediation is always negotiable and site-specific. The more defensible the characterization information, the better the chance to obtain regulatory approval.

The geophysical techniques proposed are well established in the petroleum industry where they have been applied in an extensive range of geological settings. It remains to implement the technology in the hydrogeological and subsurface contamination remediation industries.

References

Aki, K. and Richards, P.G., 1980, Quantitative Seismology: W. H. Freeman and Co., San Francisco, 932 p.

Allen, J.L. and Peddy, C.P., 1993, Amplitude variation with offset: Gulf Coast studies: SEGGeophysical Developments Series No. 4, Society of Exploration Geophysicists, Tulsa, OK, 111 p.

Bortfield, R., 1961, Approximation to the reflection and transmission coefficients of plane longitudinal and transverse waves: Geophysical Prospecting, v. 9, p. 485-502.

Castagna, J.P. and Backus, M. M., eds., 1993, Offset-dependent reflectivity - Theory and practice: SEG Investigations in Geophysics No. 8, Society of Exploration Geophysicists, Tulsa, OK, 345 p.

Castagna, J.P., Batzle, M.L., and Eastwood, R.L., 1985, Realtionship between compressional and shear-wave velocities in clastic siscate rocks, Geophysics, v. 50, p. 551-570.

Koefoed, O., 1955, On the effect of Poisson's ratios of rock strata on the reflection coefficients of plane waves: Geophysical Prospecting, p. 381-387.

Ostrander, W.J., 1984, Plane-wave reflection coefficients for gas sands at nonmormal angles of incidence: Geophysics, v. 49, p. 1637-1648

Rohay, V.L., 1994, 1994 conceptual model of the carbon tetracloride contamination in the 200west area at the Hanford Site,WHC-SD-EN-TI-248, Westinghouse Hanford Comapny, Richland, Washington.

Shuey, R.T., 1985, A simplification of the Zoeppritz equations: Geophysics, v. 50, p. 609-614.

Smith, G.C. and Gidlow, P.M., 1987, Weighted stacking for rock property estimation and detection of gas: Geophysical Prospecting, v. 35, p. 993-1014.

Verm, R. and Hilterman, F., 1995, Lithology color-coded seismic sections: The calibration of AVO crossplotting to rock properties: The Leading Edge, v. 14, n. 8, p. 847-853.

Waddell, M.G, Temples, T.J., and Domoracki, W.J., 1997, Using high-resolution reflection seismic to image free-phase DNAPLs at the M-area, Savannah River Site (Abstract): Ann. Mtg. Am. Assoc. Petroleum Geologists, Dallas, TX.

Waters, K.H., 1981, Reflection Seismology: A Tool for Energy Resource Exploration, John W, Wiley

and Sons, Inc.

Zoeppritz, K., 1919, Uber reflexion und durchgang seismischer wellen durch Unstetigkerlsflaschen: Berlin, Uber Erdbebenwellen VII B, Nachrichten der Koniglichen Gesellschaft der Wissenschaften zu Gottingen, math-phys. K1., p. 57-84.